

# Searching for turbulence models by artificial neural network

Masataka Gamahara

*Graduate School of Information Sciences,  
Tohoku University, Sendai 980-8579, Japan*

Yuji Hattori\*

*Institute of Fluid Sciences, Tohoku University, Sendai 980-8577, Japan*

(Dated: July 6, 2016)

## Abstract

Artificial neural network (ANN) is tested as a tool for finding a new subgrid model of the subgrid-scale (SGS) stress in large-eddy simulation. ANN is used to establish a functional relation between the grid-scale (GS) flow field and the SGS stress without any assumption of the form of function. Data required for training and test of ANN are provided by direct numerical simulation (DNS) of a turbulent channel flow. It is shown that ANN can establish a model similar to the gradient model. The correlation coefficients between the real SGS stress and the output of ANN are comparable to or larger than similarity models, but smaller than a two-parameter dynamic mixed model.

---

\* hattori@fmail.ifs.tohoku.ac.jp; corresponding author

## I. INTRODUCTION

Large-eddy simulation (LES) is used as an important tool of numerical simulation in a wide variety of fields where turbulent flows appear. In LES the turbulent flow fields are decomposed into resolved-scale or grid scale (GS) flow field and small-scale or subgrid-scale (SGS) fluctuations by a filtering operation. In incompressible turbulent flows the effects of the fluctuations on the GS flow field appear as the residual or SGS stress tensor. How to model the SGS stress tensor using the GS flow field is the most important issue in LES.

A number of subgrid models have been proposed since the Smagorinsky model [1]. Most of them are categorized into the Smagorinsky model, the similarity model [2], and the gradient model [3]; there are also dynamic versions of these models [4, 5] and mixed models [6]; see e.g. Lesieur and Métais [7] and Meneveau and Katz [8] for reviews. The performance of these models have been tested for some particular flows like isotropic turbulence [9] and mixing layer [10]. There is no model which is better than the other models in any flows, although the dynamic and mixed models often give more accurate results than non-dynamic models. Accuracy of the results obtained by LES is still limited as they should be interpreted with much care when experimental or DNS results are unavailable for validation; controversially, however, this is the very situation in which LES is most wanted. Thus, a new subgrid model which is much better than the existing ones should be developed. In order to pursue such a subgrid model essentially new ideas of modeling would be required; however, there has been no such idea since the prototypes of the above models were proposed.

The final goal of our research is to establish a new subgrid model for the SGS stress which performs better than the existing models. This is not an easy task since there are potentially a huge number of possibilities of modeling; in principle one can use the GS flow field in the whole domain to express the SGS stress at one point as in nonlocal methods in RANS modeling [11]; history of the GS flow field may also be used as in the Reynolds stress transport model [12]. On the other hand, the subgrid model should be based on physics of turbulence and it seems difficult to invent an essentially new model after the models listed above were established with much efforts. However, the methods of machine learning, which are extensively and successfully used in many areas, can provide us a tool for going beyond the ability of human thoughts; they are useful if they can automatically extract the essential GS flow field required for accurate modeling. In this paper, we test whether the artificial

neural network (ANN), which is one of the methods of machine learning, can be used for finding a subgrid model; it is a first step toward the above goal.

There have been many applications of ANN to turbulence modeling. Sarghini *et al.* [13] used ANN to find a relation between the GS flow field and the turbulent viscosity coefficient in the mixed model. Moreau *et al.* [14] used ANN to estimate the subgrid variance in the Cook and Riley model for a scalar field in isotropic turbulence. Recently ANN was used in Ma *et al.* [15] to find closure terms for a one-dimensional model of bubbly multiphase flows. There are many applications of ANN to combustion [16–19]; ANN is used to speed up sub-grid chemistry computations, which are usually the bottle-neck of LES of turbulent flames. In plasma turbulence Citrin *et al.* [20] used ANN to construct a model for tokamak turbulence transport model. In most of these works, however, ANN was used only as a complementary tool for optimizing model constants. Moreover, few works have dealt with SGS stress arising from convective terms, which is intrinsic to turbulence. In other words, there has been no attempt to construct an essentially new subgrid model of the SGS stress using ANN.

It should be pointed out that we aim at establishing a functional relation between the GS flow field and the SGS stress tensor without any assumption on its form; this has not been done in the past. It is contrasted to the approach by Sarghini *et al.* [13], who assumed the relation be the mixed model; their aim was to reduce the computational time by replacing the evaluation of the turbulent viscosity coefficient by ANN; the training target was the Bardina model instead of the real SGS stress. If ANN is shown to be an effective tool for turbulence modeling, it can be also applied to complex flows including compressible flows, multi-phase flows, and reactive flows, in which it is not always clear how to model the residual terms.

The paper is organized as follows. Numerical methods are described in §2; after describing the outline in §2.1, methods of DNS are detailed in §2.2; preparation of data for ANN is summarized in §2.3; methods of ANN including the choice of input variables are described in §2.4. The results are shown in §3; first, choice of input variables is discussed in §3.1; in §3.2 ANN is shown to be successful in learning the SGS stress; basic features of learning are shown in §3.3; applicability of ANN trained at a low Reynolds number to higher Reynolds numbers is tested in §3.4; finally, what kind of model ANN has established is investigated in §3.5. Summary and future works are given in §4.

## II. NUMERICAL METHODS

### A. Outline

In LES small fluctuations of a flow variable  $f$  are filtered out and we are concerned with the resolved-scale or GS flow field  $\bar{f} = \int G(\mathbf{x}')f(\mathbf{x} - \mathbf{x}')d\mathbf{x}'$ , where  $G$  is a filter function. The GS flow field is governed by the filtered Navier-Stokes equations

$$\frac{\partial \bar{u}_i}{\partial t} + \frac{\partial}{\partial x_j} (\bar{u}_i \bar{u}_j) = -\frac{\partial \bar{p}}{\partial x_i} + \frac{1}{Re} \frac{\partial^2 \bar{u}_i}{\partial x_k \partial x_k} - \frac{\partial \tau_{ij}}{\partial x_j}, \quad (1)$$

$$\frac{\partial \bar{u}_j}{\partial x_j} = 0. \quad (2)$$

Here the residual or SGS stress tensor

$$\tau_{ij} = \overline{u_i u_j} - \bar{u}_i \bar{u}_j \quad (3)$$

depends not only on the GS flow field but also on fluctuations and should be modeled using the GS flow field.

In the present study we use ANN to establish a functional relation between the GS flow field and the SGS stress tensor. First, training data for ANN are prepared using DNS data; the GS flow field are calculated from DNS data and used as input variables of ANN; the SGS stress tensor is also calculated from DNS data and used as training targets of output variables. Then, ANN is trained to establish a functional relation between the input and output variables. Finally, the ability of the trained ANN is checked using DNS data which are not used in training.

### B. Direct numerical simulation

The data used for training and test are obtained by DNS of a turbulent channel flow. We use the formulation of Kim *et al.* [21]. For spatial discretization the sixth-order accurate compact scheme is used in  $y$  which is the direction normal to the walls, while the Fourier collocation method is used in the streamwise direction  $x$  and the spanwise direction  $z$  assuming periodic boundary conditions. Non-uniform grids are adopted in  $y$  to resolve the boundary layers. The Poisson equations are solved in the Fourier space where they are decomposed into independent second-order ordinary differential equations for Fourier modes; they are also discretized by the compact scheme and solved accurately and efficiently. The friction



Reynolds number is  $Re_\tau = u_\tau \delta / \nu = 180, 400, 600$  and  $800$ , where  $u_\tau = \tau_w^{1/2}$ ,  $\tau_w = (1/Re) \frac{\partial u}{\partial y}$ , and  $\delta = 1$  is the channel half-width. The size of numerical domain  $L_x \times L_y \times L_z$ , the grid spacings in wall unit  $\Delta x^+$ ,  $\Delta y_{\max}^+$ , and  $\Delta z^+$ , and the number of grid points  $N_x \times N_y \times N_z$  are listed in Table I.

TABLE I: Parameter values of DNS.

$Re_\tau$	$L_x$	$L_y$	$L_z$	$\Delta x^+$	$\Delta y_{\max}^+$	$\Delta z^+$	$N_x \times N_y \times N_z$
180	$4\pi$	2	$2\pi$	11.8	5.4	7.1	$192 \times 128 \times 160$
400	$2\pi$	2	$\pi$	9.8	7.9	4.9	$256 \times 192 \times 256$
600	$2\pi$	2	$\pi$	7.4	8.1	3.7	$512 \times 256 \times 512$
800	$\pi$	2	$\pi$	6.5	7.7	3.3	$384 \times 384 \times 768$

Validity of DNS is checked in Fig. 1. The mean flow has a wall-law region and log-law region (Fig. 1a). Figure 1(b) shows fine vortical structures visualized by the iso-surface of the second invariant of the deformation tensor, which have been observed in previous works [22–24].

### C. Preparing data for training and test

The data obtained by DNS are used both for training and for test. In training field data obtained by DNS are filtered as normally done in LES to give the GS flow field on coarse grids, which are used as input variables; in the present study we use the top-hat filter function. The SGS stress is also calculated using the DNS data and is used as training targets of output variables. The values of the filter size and the number of grid points of the coarse grids are listed in Table II; for the most part they are set to the underlined parameter values  $Re_\tau = 180, (\overline{\Delta x^+}, \overline{\Delta y_{\max}^+}, \overline{\Delta z^+}) = (35.3, 9.9, 17.7)$ . The components of SGS stress tensor averaged in the streamwise and spanwise directions are shown in Fig. 2, where the rms amplitudes are also shown. They are in good agreement with the previous results [21].

The amount of data used for training is rather small; typically six positions in the streamwise direction are randomly chosen and the data on the corresponding planes parallel to the  $yz$  plane are used for training. The whole data are used for test of the trained ANN.

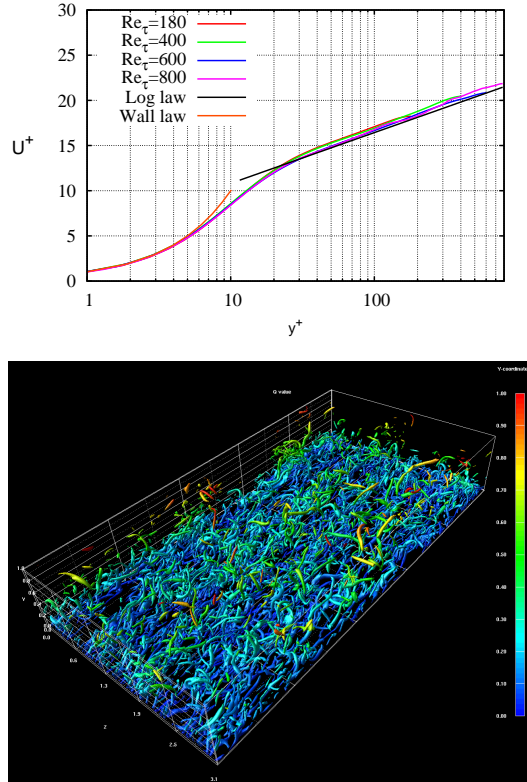


FIG. 1: Results of DNS of channel flow. (a) Mean flow at  $Re_\tau = 180, 400, 600,$  and  $800$ ; (b) vortical structures shown by iso-surface of the second invariant  $Q$  of the deformation tensor.  $Re_\tau = 400, Q = 0.03$ .

#### D. Artificial neural network (ANN)

A feedforward neural network is employed in establishing a functional relation between the GS flow field and the SGS stress tensor. Figure 3 shows the schematic diagram of ANN and a single neuron. Let us consider ANN which consists of  $L$  layers. A single neuron of the  $l$ -th layer receives a set of inputs  $\{X_j^{(l-1)}\}$  and then outputs  $X_i^{(l)}$  which is calculated as

$$X_i^{(l)} = \mathcal{B} \left( s_i^{(l)} + b_i^{(l)} \right), \quad (4)$$

$$s_i^{(l)} = \sum_j W_{ij}^{(l)} X_j^{(l-1)}, \quad (5)$$

where  $\mathcal{B}$  is the activation function,  $b_i^{(l)}$  is the bias parameter, and  $W_{ij}^{(l)}$  is the weight. The bias parameters and the weights are corrected iteratively so that the final output  $X^{(L)}$  approximates well the given SGS stress. The data of the first layer  $\{X_j^{(1)}\}$  are given by the GS flow field.

TABLE II: Parameter values for filtering. Filter size and number of grid points.

$Re_\tau$	$\overline{\Delta x}^+$	$\overline{\Delta y}_{\max}^+$	$\overline{\Delta z}^+$	$N_x \times N_y \times N_z$
180	41.7	15.6	23.6	$48 \times 48 \times 48$
	43.5	14.5	21.7	$52 \times 52 \times 52$
	<u>35.3</u>	<u>9.9</u>	<u>17.7</u>	<u><math>64 \times 64 \times 64</math></u>
	23.6	6.0	11.8	$96 \times 96 \times 96$
400	39.3	22.0	19.6	$64 \times 64 \times 64$
	34.3	17.9	17.5	$72 \times 72 \times 72$
	29.9	15.3	15.0	$84 \times 84 \times 84$
	26.2	13.3	13.1	$96 \times 96 \times 96$
600	29.5	33.0	14.7	$128 \times 64 \times 128$
	26.2	26.9	13.1	$144 \times 72 \times 144$
	22.4	23.0	11.2	$168 \times 84 \times 168$
	19.6	19.9	9.8	$192 \times 96 \times 192$
800	26.2	10.9	13.1	$96 \times 256 \times 192$
	19.6	10.9	9.8	$128 \times 256 \times 256$
	13.1	10.9	6.5	$192 \times 256 \times 384$

In the present study ANN consists of three layers: the input, hidden, and output layers. For simplicity, each independent component of the SGS stress tensor is dealt with separately; in other words, six ANNs are trained to approximate all components of the SGS stress tensor. This point will be discussed from the viewpoint of symmetry in the final section. The activation function is the sigmoid function  $\mathcal{B}(z) = 1/(1 + e^{-\alpha z})$ . The back propagation is used as a method for training which optimizes the bias parameters and weights iteratively to minimize the difference between the output and the given SGS stress  $\sum |X^{(L)} - \tau_{ij}|^2$ . The number of neurons of the input layer depends on the choice of input variables as described below, while the output layer consists of a single neuron. The number of neurons of the hidden layer is 100 unless stated explicitly, while the dependence on it is checked in Sec. III C.

We should be careful in choosing the input variables since it is important for effective

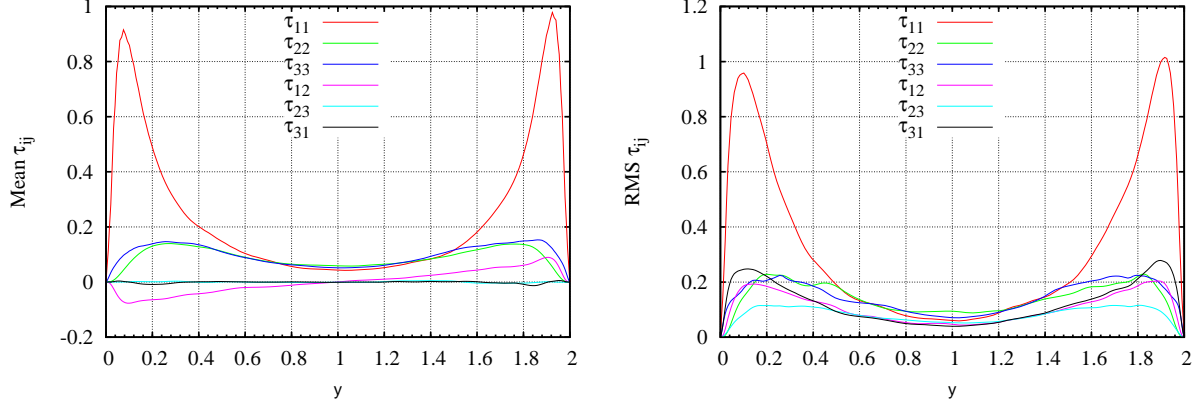


FIG. 2: Distributions of SGS stress tensor  $\tau_{ij}$  averaged in streamwise and spanwise directions ( $xz$ -plane).  $Re_\tau = 180$ ,  $(\overline{\Delta x^+}, \overline{\Delta y_{\max}^+}, \overline{\Delta z^+}) = (35.3, 9.9, 17.7)$ . (Left) Average and (right) rms amplitude of fluctuation.

and successful learning. Although there are many possibilities for the combination of input variables, we limit ourselves to pointwise correspondence between the input and output variables; namely, in order to approximate the SGS stress at one point the GS data at the same point are used as input variables. We test four sets of input variables: (i)  $\{\mathbf{S}, y\}$ ; (ii)  $\{\mathbf{S}, \boldsymbol{\Omega}, y\}$ ; (iii)  $\{\nabla \bar{\mathbf{u}}, y\}$ ; (iv)  $\{\nabla \bar{\mathbf{u}}\}$ , where  $\mathbf{S} = [\nabla \bar{\mathbf{u}} + (\nabla \bar{\mathbf{u}})^T]/2$  and  $\boldsymbol{\Omega} = [\nabla \bar{\mathbf{u}} - (\nabla \bar{\mathbf{u}})^T]/2$ . The first set can give the Smagorinsky model  $\tau_{ij} = -2C_S \bar{\Delta}^2 (2S_{kl}S_{kl})^{1/2} S_{ij} + (1/3)\tau_{kk}\delta_{ij}$ , while the position  $y$  is included to take account of possible dependence on the wall-normal direction. The GS vorticity is added in the second set since it improves the accuracy of the SGS model in some flows [25]. The third set is equivalent to the second one in the sense that  $\nabla \bar{\mathbf{u}} = \mathbf{S} + \boldsymbol{\Omega}$ ; in practice, however, the results of learning can be different. The last set is included to check the role of the position  $y$ .

### III. RESULTS

#### A. Choice of input variables

First, we investigate which set of input variables results in successful learning. Figure 4 shows correlation coefficients between the SGS stress  $\tau_{ij}^{(DNS)}$  calculated using DNS data and  $\tau_{ij}^{(ANN)}$  predicted by trained ANN for the four sets of input variables for  $Re_\tau = 180$ ,  $(\overline{\Delta x^+}, \overline{\Delta y_{\max}^+}, \overline{\Delta z^+}) = (35.3, 9.9, 17.7)$ . The correlation coefficients are calculated by

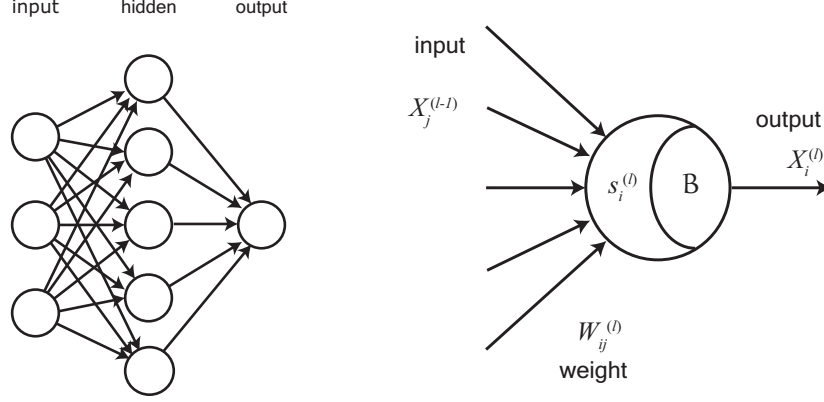


FIG. 3: Schematic diagram of artificial neural network (ANN). (Left) Network structure; (right) single neuron.

integrating in  $x$  and  $z$  directions

$$\text{C.C.}(y) = \frac{\left\langle \left( \tau_{ij}^{(DNS)} - \langle \tau_{ij}^{(DNS)} \rangle_{xz} \right) \left( \tau_{ij}^{(ANN)} - \langle \tau_{ij}^{(ANN)} \rangle_{xz} \right) \right\rangle_{xz}}{\left[ \left\langle \left( \tau_{ij}^{(DNS)} - \langle \tau_{ij}^{(DNS)} \rangle_{xz} \right)^2 \right\rangle_{xz} \right]^{1/2} \left[ \left\langle \left( \tau_{ij}^{(ANN)} - \langle \tau_{ij}^{(ANN)} \rangle_{xz} \right)^2 \right\rangle_{xz} \right]^{1/2}},$$

$$\langle f \rangle_{xz} = \frac{1}{L_x L_z} \int_0^{L_x} dx \int_0^{L_z} dz f(x, y, z).$$

High correlation implies successful learning. It is seen that learning is most successful when  $\{\nabla \bar{\mathbf{u}}, y\}$  is used as input variables as the averaged correlation coefficient  $\overline{\text{C.C.}} = (1/L_y) \int_0^{L_y} dy \text{C.C.}(y)$  exceeds 0.7 for all six components as shown in Table III, although  $\{\nabla \bar{\mathbf{u}}\}$  gives comparable success; the difference of the correlation coefficients between the two sets is  $0 \sim 4\%$ . Thus the distance from the wall is not important very much. The Smagorinsky type  $\{\mathbf{S}, y\}$  gives poor results as the averaged correlation coefficient exceeds 0.7 for only one component  $\tau_{11}$ ; the correlation coefficients of the other components are small in the entire region besides that it is large for  $\tau_{31}$  near the wall. This result is reasonable since it is known that the eddy-viscosity type model has little correlation with the real SGS stress [26]. There is a little improvement by including  $\boldsymbol{\Omega}$  as the set  $\{\mathbf{S}, \boldsymbol{\Omega}, y\}$  gives three correlation coefficients which exceed 0.7; the correlation coefficients of  $\tau_{33}$ ,  $\tau_{23}$ , and  $\tau_{31}$  are small in the central region where both the average and rms amplitude of these components are small. However, it should be pointed out that the set  $\{\mathbf{S}, \boldsymbol{\Omega}, y\}$  is not good as  $\{\nabla \bar{\mathbf{u}}, y\}$ , although the two sets have essentially the same degree of freedom.

Among the components of the SGS stress tensor  $\tau_{11}$  is the easiest component for regression

as all four sets give correlation coefficients larger than 0.7; this is because  $\tau_{11}$  is largest in magnitude (Fig. 2). On the other hand,  $\tau_{23}$  and  $\tau_{31}$ , of which averages are zero and amplitudes are small (Fig. 2), are difficult to be approximated as the correlation coefficients are small for both  $\{\mathcal{S}, y\}$  and  $\{\mathcal{S}, \Omega, y\}$ . In the rest of the paper the set of input variables is fixed to  $\{\nabla \bar{\mathbf{u}}, y\}$ .

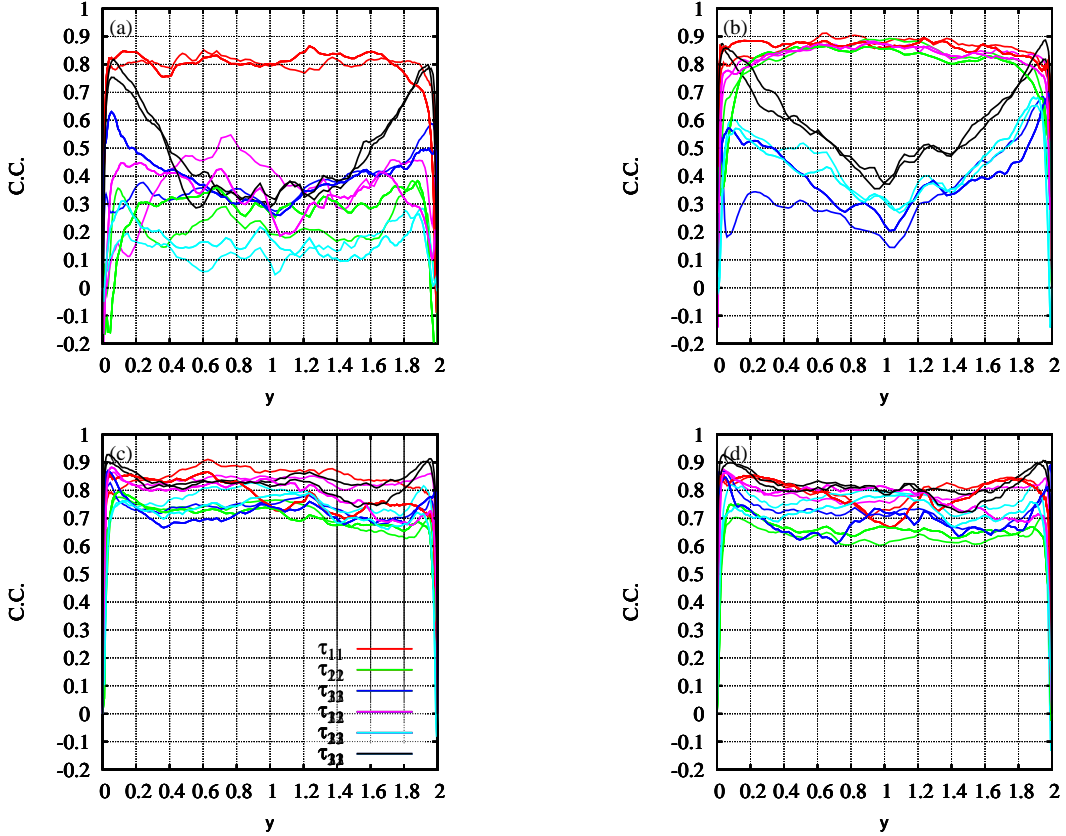


FIG. 4: Correlation coefficients between the SGS stress  $\tau_{ij}^{(DNS)}$  calculated using DNS data and  $\tau_{ij}^{(ANN)}$  predicted by trained ANN. Correlation coefficients are averaged in streamwise and spanwise directions ( $xz$ -plane).  $Re_\tau = 180$ ,  $(\overline{\Delta x^+}, \overline{\Delta y_{\max}^+}, \overline{\Delta z^+}) = (35.3, 9.9, 17.7)$ . (a)  $\{\mathcal{S}, y\}$ , (b)  $\{\mathcal{S}, \Omega, y\}$ , (c)  $\{\nabla \bar{\mathbf{u}}, y\}$ , (d)  $\{\nabla \bar{\mathbf{u}}\}$ .

## B. How successful is the learning?

Next, we look into some details of the learning results for  $Re_\tau = 180$ ,  $(\overline{\Delta x^+}, \overline{\Delta y_{\max}^+}, \overline{\Delta z^+}) = (35.3, 9.9, 17.7)$ . Figures 5 and 6 compares the distributions of the SGS stress obtained by filtering DNS data,  $\tau_{ij}^{(DNS)}$ , and that predicted by trained ANN,  $\tau_{ij}^{(ANN)}$ . We choose the

TABLE III: Correlation coefficients between the SGS stress  $\tau_{ij}^{(DNS)}$  calculated using DNS data and  $\tau_{ij}^{(ANN)}$  predicted by trained ANN. Correlation coefficients are averaged in the whole domain.

Input variables	$\tau_{11}$	$\tau_{22}$	$\tau_{33}$	$\tau_{12}$	$\tau_{23}$	$\tau_{31}$
$\{\mathbf{S}, y\}$	0.793	0.292	0.390	0.320	0.148	0.489
$\{\mathbf{S}, \mathbf{\Omega}, y\}$	0.776	0.769	0.344	0.773	0.368	0.524
$\{\nabla \bar{\mathbf{u}}, y\}$	0.804	0.713	0.728	0.791	0.730	0.821
$\{\nabla \bar{\mathbf{u}}\}$	0.767	0.670	0.710	0.776	0.720	0.820

plane  $y = 0.1$  where the rms amplitudes of all components are nearly largest. The values of each component are normalized to be in  $[0, 1]$ . ANN is seen to reproduce fairly well the patterns in the distributions of DNS. Good agreement is also observed for the average (Fig. 7) and rms amplitude (Fig. 8) of each component. The learning is successful.

### C. Basic features of learning

In this subsection we show some features of learning by ANN which can be important in efficient applications. Table IV confirms that there is no significant dependence on the data set used in training. Five different data sets are tested. The difference between the correlation coefficients and the average is less than 0.043.

Figure 9 is a magnified view of Fig. 4 near the wall. It shows that the correlation coefficients are small in the near wall region  $y^+ < 10$ , which consists of the viscous sublayer and a part of the buffer layer; it is reasonable since the flow field is not fully turbulent in this region. Outside this region, however, the correlation coefficients do not depend on the position  $y$  significantly.

Table V shows how many neurons are needed for successful learning. In this table  $n$  is the number of neurons in the hidden layer. In general, approximation by ANN becomes more accurate by increasing  $n$  with the expense of computational time. It is seen that the correlation coefficients increase with  $n$ , but the increase is slow for  $n \geq 10$ . All correlation coefficients exceed 0.7 when  $n \geq 50$ . Figure 10 shows how the difference between DNS and

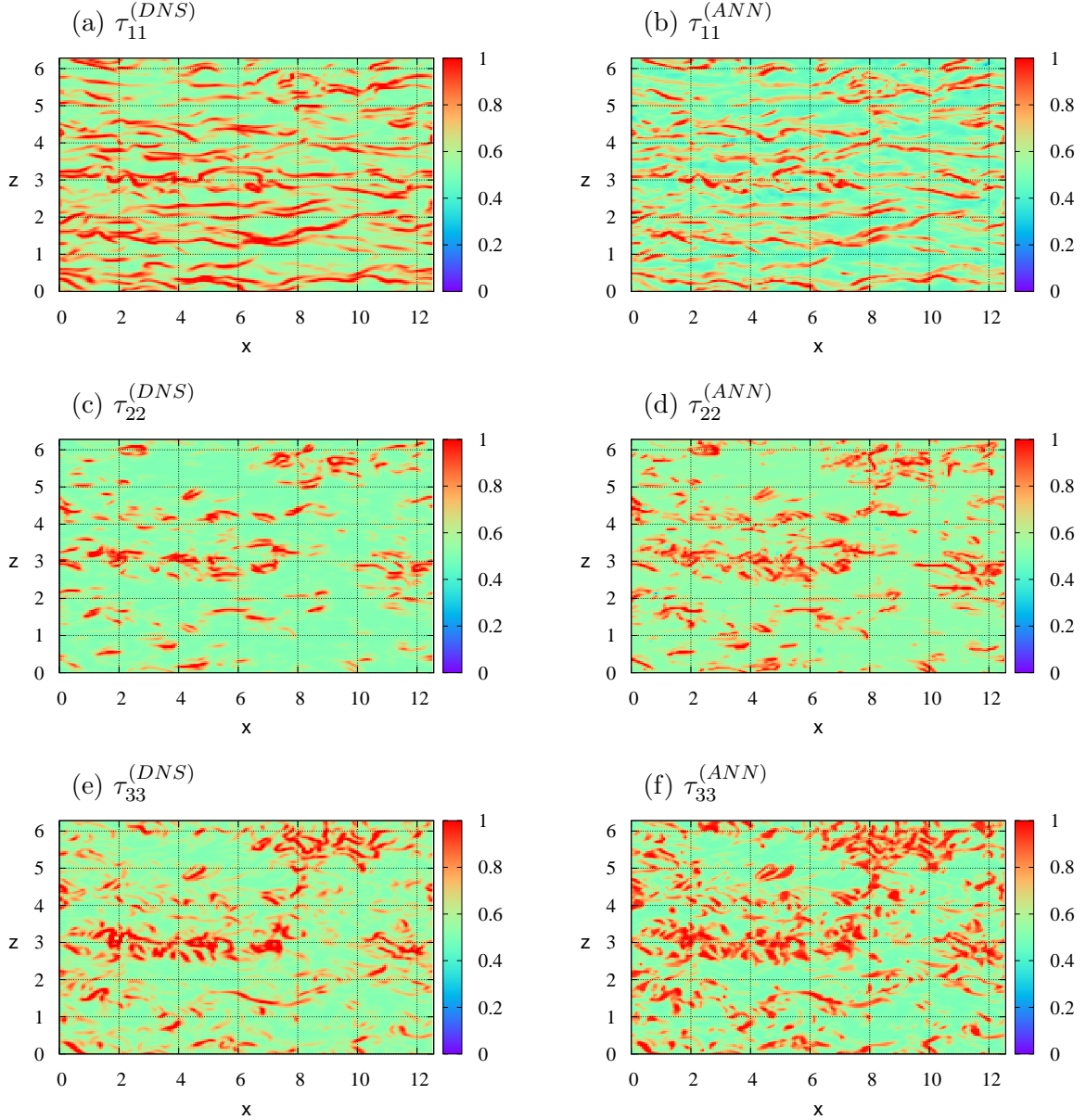


FIG. 5: Spatial distributions of SGS stress tensor at  $y = 0.1$ . Comparison between  $\tau_{ij}^{(DNS)}$  and  $\tau_{ij}^{(ANN)}$ . Diagonal components.  $Re_\tau = 180$ ,  $(\overline{\Delta x}^+, \overline{\Delta y}_{\max}^+, \overline{\Delta z}^+) = (35.3, 9.9, 17.7)$ .

ANN decays with the number of iterations in training. As the number of neurons increases the rate of decay increases and the final error after 1000 iterations of learning decreases. On the other hand, the time required for ANN calculation increases with  $n$ . Thus the choice of  $n$  should be made taking account of the accuracy of approximation as well as the calculation time.

Figure 11 shows the overall correlation coefficients as a function of the averaged filter



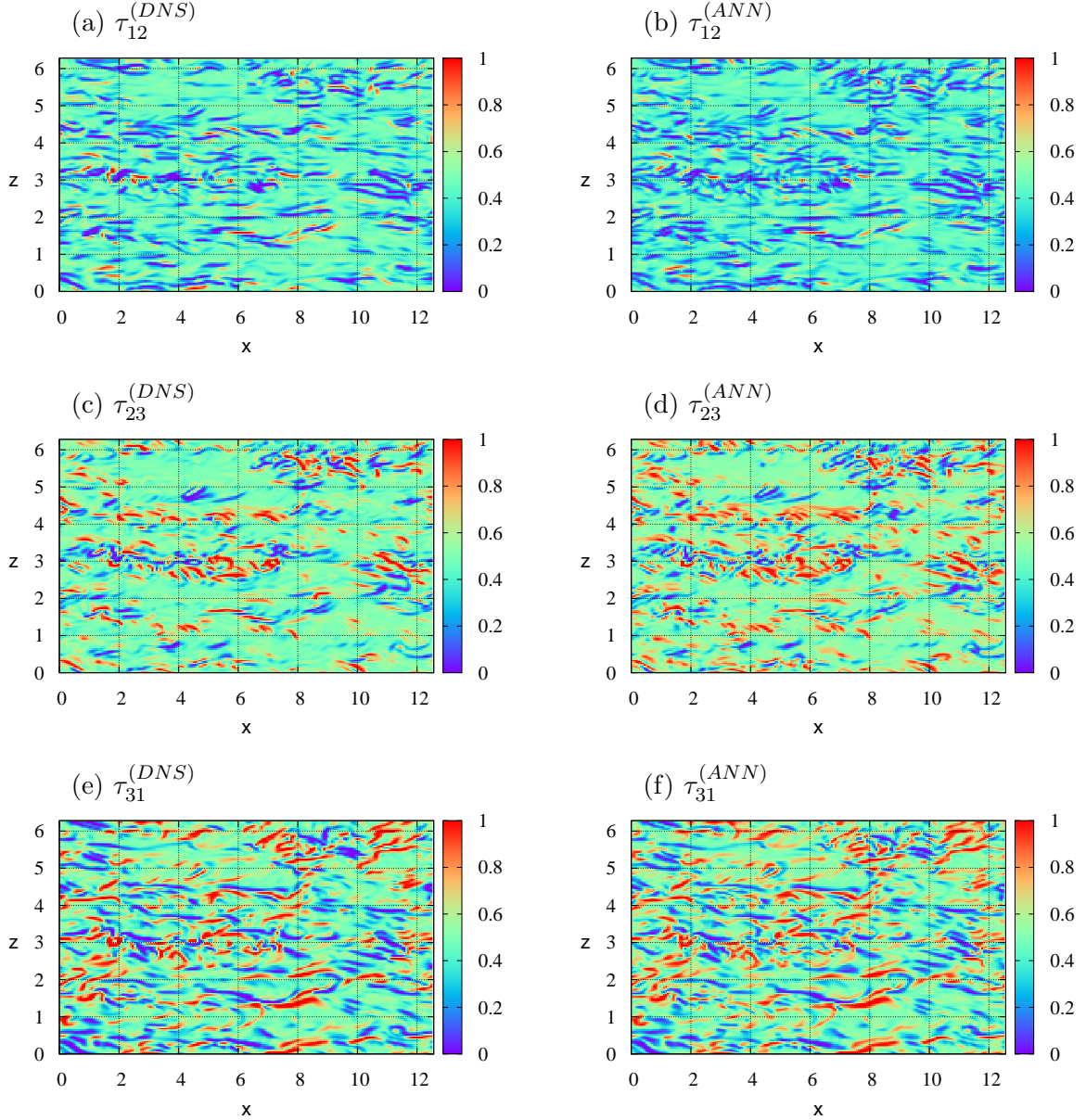


FIG. 6: Spatial distributions of SGS stress tensor at  $y = 0.1$ . Same as in Fig. 5 but for off-diagonal components.

size  $\bar{\Delta}^+ = \left( \overline{\Delta x^+} \overline{\Delta y_{\max}^+} \overline{\Delta z^+} \right)^{1/3}$  for various Reynolds numbers. It is seen that learning is successful for  $\bar{\Delta}^+ \lesssim 20$ , which corresponds to 3  $\sim$  4 times grid spacing. The correlation coefficients decrease quickly as the filter size becomes large. Thus there is a limitation for the filter size. There is little dependence on the Reynolds number, although the correlation coefficient is larger for  $Re_\tau = 400$  than the other three cases.

TABLE IV: Correlation coefficients between the SGS stress  $\tau_{ij}^{(DNS)}$  calculated using DNS data and  $\tau_{ij}^{(ANN)}$  predicted by trained ANN. Dependence on training data set. Correlation coefficients are averaged in the whole domain.

data set	$\tau_{11}$	$\tau_{22}$	$\tau_{33}$	$\tau_{12}$	$\tau_{23}$	$\tau_{31}$
1st	0.796	0.696	0.750	0.760	0.731	0.826
2nd	0.802	0.711	0.693	0.753	0.734	0.784
3rd	0.835	0.715	0.743	0.834	0.750	0.832
4th	0.768	0.709	0.708	0.792	0.732	0.826
5th	0.816	0.732	0.747	0.815	0.703	0.839
Average	0.804	0.713	0.728	0.791	0.730	0.821

TABLE V: Correlation coefficients between  $\tau_{ij}^{(DNS)}$  and  $\tau_{ij}^{(ANN)}$ . Dependence on the number of neurons. Correlation coefficients are averaged in the whole domain.

$n$	$\tau_{11}$	$\tau_{22}$	$\tau_{33}$	$\tau_{12}$	$\tau_{23}$	$\tau_{31}$
2	0.677	0.487	0.486	0.366	0.398	0.547
5	0.752	0.671	0.674	0.593	0.604	0.710
10	0.742	0.672	0.717	0.779	0.711	0.801
25	0.782	0.684	0.739	0.807	0.736	0.807
50	0.806	0.709	0.739	0.796	0.739	0.812
100	0.827	0.711	0.739	0.788	0.736	0.816

#### D. Applicability to higher Reynolds numbers

LES is usually used for high Reynolds number flows which are not accessible by DNS. Thus when we think of applying ANN to LES of high Reynolds number flows, no training data are available from DNS. In this regard, it is of importance to check whether ANN trained at low Reynolds numbers is useful at high Reynolds numbers. This is checked applying ANN trained at  $Re_\tau = 180$  to predicting the SGS stress tensor at  $Re_\tau = 400$ .

Figure 12 compares the distribution of  $\tau_{11}^{(DNS)}$  obtained by filtering DNS data of  $Re_\tau = 400$  with filter size  $(\overline{\Delta x}^+, \overline{\Delta y}_{\max}^+, \overline{\Delta z}^+) = (34.3, 17.9, 17.5)$  and  $\tau_{11}^{(ANN)}$  predicted by ANN trained at  $Re_\tau = 180$  with filter size  $(\overline{\Delta x}^+, \overline{\Delta y}_{\max}^+, \overline{\Delta z}^+) = (35.3, 9.9, 17.7)$ . Although there is some difference in the magnitude, the spatial patterns in DNS data are reproduced by ANN. The correlation coefficients between DNS and ANN are larger than 0.7 (Table VI). These results support that it is possible to use ANN trained at low Reynolds numbers for LES at high Reynolds numbers.

TABLE VI: Correlation coefficients between  $\tau_{ij}^{(DNS)}$  obtained by filtering DNS data of  $Re_\tau = 400$  with filter size  $(\overline{\Delta x}^+, \overline{\Delta y}_{\max}^+, \overline{\Delta z}^+) = (34.3, 17.9, 17.5)$  and  $\tau_{ij}^{(ANN)}$  predicted by ANN trained at  $Re_\tau = 180$  with filter size  $(\overline{\Delta x}^+, \overline{\Delta y}_{\max}^+, \overline{\Delta z}^+) = (35.3, 9.9, 17.7)$ .

Correlation coefficients are averaged in the whole domain.

$\tau_{11}$	$\tau_{22}$	$\tau_{33}$	$\tau_{12}$	$\tau_{23}$	$\tau_{31}$
0.707	0.744	0.734	0.743	0.768	0.769

### E. What ANN has learned?

Finally, we investigate what kind of model ANN has established. First, we identify and eliminate members of the input variables which are not required for ANN approximation for each component of the SGS stress tensor. This is done by removing components of  $\nabla \bar{\mathbf{u}}$  one by one and checking whether the correlation coefficients become much smaller than before. Table VII shows the results; the members of the input variables required for achieving high correlation coefficients are marked by circles. The values of correlation coefficients with the reduced numbers of input variables are shown in the first row of Table VIII. They are larger than those obtained with the full members of  $\{\nabla \bar{\mathbf{u}}, y\}$  (Table III). Thus the results of learning are improved by eliminating irrelevant components.

Next, we infer the model ANN has produced. The above results imply that

$$\tau_{ij} = f\left(\frac{\partial \bar{u}_i}{\partial x}, \frac{\partial \bar{u}_i}{\partial z}, \frac{\partial \bar{u}_j}{\partial x}, \frac{\partial \bar{u}_j}{\partial z}, y\right), \quad (6)$$

TABLE VII: Input variables required for accurate prediction by ANN.

	$\frac{\partial u}{\partial x}$	$\frac{\partial u}{\partial y}$	$\frac{\partial u}{\partial z}$	$\frac{\partial v}{\partial x}$	$\frac{\partial v}{\partial y}$	$\frac{\partial v}{\partial z}$	$\frac{\partial w}{\partial x}$	$\frac{\partial w}{\partial y}$	$\frac{\partial w}{\partial z}$
$\tau_{11}$	○		○						
$\tau_{22}$				○		○			
$\tau_{33}$							○		○
$\tau_{12}$	○		○						
$\tau_{23}$				○		○	○		○
$\tau_{31}$	○		○				○		○

which reminds us of the gradient model

$$\tau_{ij} = \frac{\bar{\Delta}^2}{12} \frac{\partial \bar{u}_i}{\partial x_k} \frac{\partial \bar{u}_j}{\partial x_k}. \quad (7)$$

We prefer the following form

$$\tau_{ij} = \sum_{k=1}^3 \frac{\bar{\Delta}_k^2}{12} \frac{\partial \bar{u}_i}{\partial x_k} \frac{\partial \bar{u}_j}{\partial x_k}, \quad (8)$$

since the grid spacings in  $y$  direction are much smaller than the other two directions.

Figure 13 shows the distribution of  $\tau_{11}$  obtained by the gradient model. It is similar to not only  $\tau_{11}^{(DNS)}$  but also  $\tau_{11}^{(ANN)}$  (Fig. 5). In Table VIII the correlation between the gradient model (8) and DNS is high and comparable to the correlation between ANN and DNS. The correlation coefficients between the gradient model and ANN are a bit smaller than those in the other two rows, but still large. Thus, ANN has established a model which is similar to the gradient model.

#### IV. CONCLUDING REMARKS

We have shown that ANN can establish a functional relation between the GS flow field and the SGS stress tensor in LES. Using DNS data of a turbulent channel flow as training data, ANN was trained by back propagation. Then the ability of the trained ANN was tested using DNS data which were not used in training. Learning was most successful when  $\{\nabla \bar{\mathbf{u}}, y\}$  was used as a set of the input variables; the correlation coefficients between the

TABLE VIII: Correlation coefficients between (top)  $\tau_{ij}^{(DNS)}$  and  $\tau_{ij}^{(ANN)}$  with reduced number of input variables, (middle) the gradient model and  $\tau_{ij}^{(DNS)}$ , and (bottom) the gradient model and  $\tau_{ij}^{(ANN)}$ . Correlation coefficients are averaged in the whole domain.

$$Re_\tau = 180, (\overline{\Delta x^+}, \overline{\Delta y_{\max}^+}, \overline{\Delta z^+}) = (35.3, 9.9, 17.7).$$

Case	$\tau_{11}$	$\tau_{22}$	$\tau_{33}$	$\tau_{12}$	$\tau_{23}$	$\tau_{31}$
reduced input variables	0.863	0.769	0.793	0.848	0.793	0.856
gradient model vs. DNS	0.847	0.729	0.737	0.841	0.703	0.853
gradient model vs. ANN	0.651	0.675	0.634	0.758	0.664	0.640

SGS stress tensor obtained by filtering DNS data and that predicted by ANN exceeded 0.7. The spatial distribution of the SGS stress tensor predicted by ANN was in good agreement with that obtained by filtering DNS data. It is most likely that ANN has established a model close to the gradient model.

It should be pointed out that learning was successful only when the filter size was small:  $\overline{\Delta}^+ \lesssim 20$ . For this small filter size the SGS Reynolds stress term is so small that the SGS stress is close to the sum of the Leonard term and the cross-stress term, which can be approximated by the gradient model. Therefore, the present results are quite reasonable. However, it should be stressed that ANN has succeeded in establishing a functional relation between the GS flow field and the SGS stress without any assumption on the form of function. We also remark that the values of correlation coefficients between DNS and ANN obtained in the present study are comparable to or even larger than those for similarity models [26, 27] but smaller than those for a dynamic two-parameter mixed model [28], which implies that ANN is a promising tool for searching for new turbulence models and should be improved.

In the present study we have not taken care of symmetry of the SGS stress tensor; each component of the tensor is trained separately. If the fluctuations are statistically isotropic, however, the turbulence model should be also isotropic; training is required for only one diagonal component and one off-diagonal component of the SGS stress tensor, while the two are related through the incompressibility condition. In the present study, however, the grid spacings and the filter size differ depending on the direction; this is one of the reasons

why each component of the SGS stress tensor is trained independently. It should be noted that it is important to take account of symmetry when we formulate a trained ANN into a turbulence model.

Although we have obtained some successful results with ANN, several problems should be solved in order to find a new turbulence model better than the existing ones, which is our final goal. We would like to find a model which works well even when the filter size is much larger than the grid size. However, it may be impossible to have high correlation of the SGS stress tensor between ANN and DNS for large filter size since SGS fluctuations involve a wide range of length scales and are inevitably large. In this regard, one way to proceed is to allow a certain level of errors, which can be incorporated in other methods of machine learning like support vector machine/regression. Another way is to replace the training target or output variable; in the present study we chose the SGS stress tensor as the output variable, but it can be other quantities like the rate of production of residual energy or SGS dissipation, which is important in the energy transfer between GS and SGS scales.

ANN itself can be also improved. There are a number of possibilities in the choice of input variables. In the present study the input variables were chosen taking account of the Smagorinsky model, but it can be replaced by the similarity model and we can include doubly-filtered variables in the input variables. We may include all data if the ability of ANN allows it. In this regard, tuning of ANN would be also important; the number of layers may be increased as we see the remarkable success of deep learning.

## ACKNOWLEDGMENTS

Numerical calculations were performed on the Altix UV1000 and UV2000 at the Advanced Fluid Information Research Center, Institute of Fluid Science, Tohoku University.

- 
- [1] J. Smagorinsky, General circulation experiments with the primitive equations, *Mon. Weather Rev.* **91**, 99 (1963).
  - [2] J. Bardina, J. H. Ferziger, and W. C. Reynolds, Improved turbulence models based on LES

- of homogeneous incompressible turbulent flows, Rep. TF-19. Department of Mechanical Engineering, Stanford (1984).
- [3] R. A. Clark, J. H. Ferziger, and W. C. Reynolds, Evaluation of subgrid-scale models using an accurately simulated turbulent flow, *J. Fluid Mech.* **91**, 1 (1979).
  - [4] M. Germano, Turbulence: the filtering approach, *J. Fluid Mech.* **238**, 325 (1992).
  - [5] B. Vreman, B. Geurts, and H. Kuerten, Large eddy simulation of the temporal mixing layer using the Clark model, *Theor. Comput. Fluid Dyn.* **8**, 309 (1996).
  - [6] Y. Zang, R. L. Street, and J. R. Koseff, A dynamic mixed subgrid-scale model and its application to turbulent recirculating flows, *Phys. Fluids A* **5**, 3186 (1993).
  - [7] M. Lesieur and O. Métais, New trends in large-eddy simulations of turbulence, *Annu. Rev. Fluid Mech.* **28**, 45 (1996).
  - [8] C. Meneveau and J. Katz, Scale-invariance and turbulence models for large-eddy simulation, *Annu. Rev. Fluid Mech.* **32**, 1 (2000).
  - [9] C. Fureby, G. Tabor, H. G. Weller, and A. D. Gosman, A comparative study of subgrid scale models in homogeneous isotropic turbulence, *Phys. Fluids* **9**, 1416 (1997).
  - [10] B. Vreman, B. Geurts, and H. Kuerten, Large-eddy simulation of the turbulent mixing layer, *J. Fluid Mech.* **339**, 357 (1997).
  - [11] F. Hamba, Nonlocal analysis of the Reynolds stress in turbulent shear flow, *Phys. Fluids* **17** 115102 (2005).
  - [12] S. B. Pope, *Turbulent Flows*, (Cambridge University Press, New York, 2002), Chap. 11.
  - [13] F. Sarghini, G. de Felice, and S. Santini, Neural networks based subgrid scale modeling in large eddy simulations, *Comput. Fluids* **32**, 97 (2003).
  - [14] A. Moreau, O. Teytaud, and J. P. Bertoglio, Optimal estimation for large-eddy simulation of turbulence and application to the analysis of subgrid models, *Phys. Fluids* **18** 105101 (2006).
  - [15] M. Ma, J. Lu, and G. Tryggvason Using statistical learning to close two-fluid multiphase flow equations for a simple bubbly system, *Phys. Fluids* **27** 092101 (2015).
  - [16] M. Ihme, C. Schmitt, and H. Pitsch, Optimal artificial neural networks and tabulation methods for chemistry representation in LES of a bluff-body swirl-stabilized flame, *Proc. Combust. Inst.* **32**, 1527 (2009).
  - [17] B. A. Sen and S. Menon, Turbulent premixed flame modeling using artificial neural networks based chemical kinetics, *Proc. Combust. Inst.* **32**, 1605 (2009).

- [18] B. A. Sen, E. R. Hawkes, and S. Menon, Large eddy simulation of extinction and reignition with artificial neural networks based chemical kinetics, *Combust. Flame* **157**, 566 (2010).
- [19] M.D. Emami and A. E. Fard, Laminar flamelet modeling of a turbulent CH<sub>4</sub>/H<sub>2</sub>/N<sub>2</sub> jet diffusion flame using artificial neural networks, *Appl. Math. Model.* **36**, 2082 (2012).
- [20] J. Citrin *et al.*, Real-time capable first principle based modelling of tokamak turbulent transport, *Nucl. Fusion* **55** 092001 (2015).
- [21] J. Kim, P. Moin and R. Moser, Turbulence statistics in fully developed channel flow at a low Reynolds number, *J. Fluid Mech.* **177**, 133 (1987).
- [22] H. Abe, H. Kawamura, and Y. Matsuo, Direct Numerical Simulation of a Fully Developed Turbulent Channel Flow With Respect to the Reynolds Number Dependence, *Trans. ASME J. Fluids Eng.* **123** 382 (2001).
- [23] W. Schoppa and F. Hussain, Coherent structure generation in near-wall turbulence, *J. Fluid Mech.* **453**, 57 (2002).
- [24] B. Ganapathisubramani, E. K. Longmire, and I. Marusic, Experimental investigation of vortex properties in a turbulent boundary layer, *Phys. Fluids* **18** 055105 (2006).
- [25] H. Kobayashi, The subgrid-scale models based on coherent structures for rotating homogeneous turbulence and turbulent channel flow, *Phys. Fluids* **17** 045104 (2005).
- [26] S. Liu, C. Meneveau, and J. Katz, On the properties of similarity subgrid-scale models as deduced from measurements in a turbulent jet, *J. Fluid Mech.* **275**, 83 (1994).
- [27] K. Horiuti, The role of the Bardina model in large eddy simulation of turbulent channel flow, *Phys. Fluids* **A1** 426 (1989).
- [28] K. Horiuti, A new dynamic two-parameter mixed model for large-eddy simulation, *Phys. Fluids* **9** 3443 (1997).



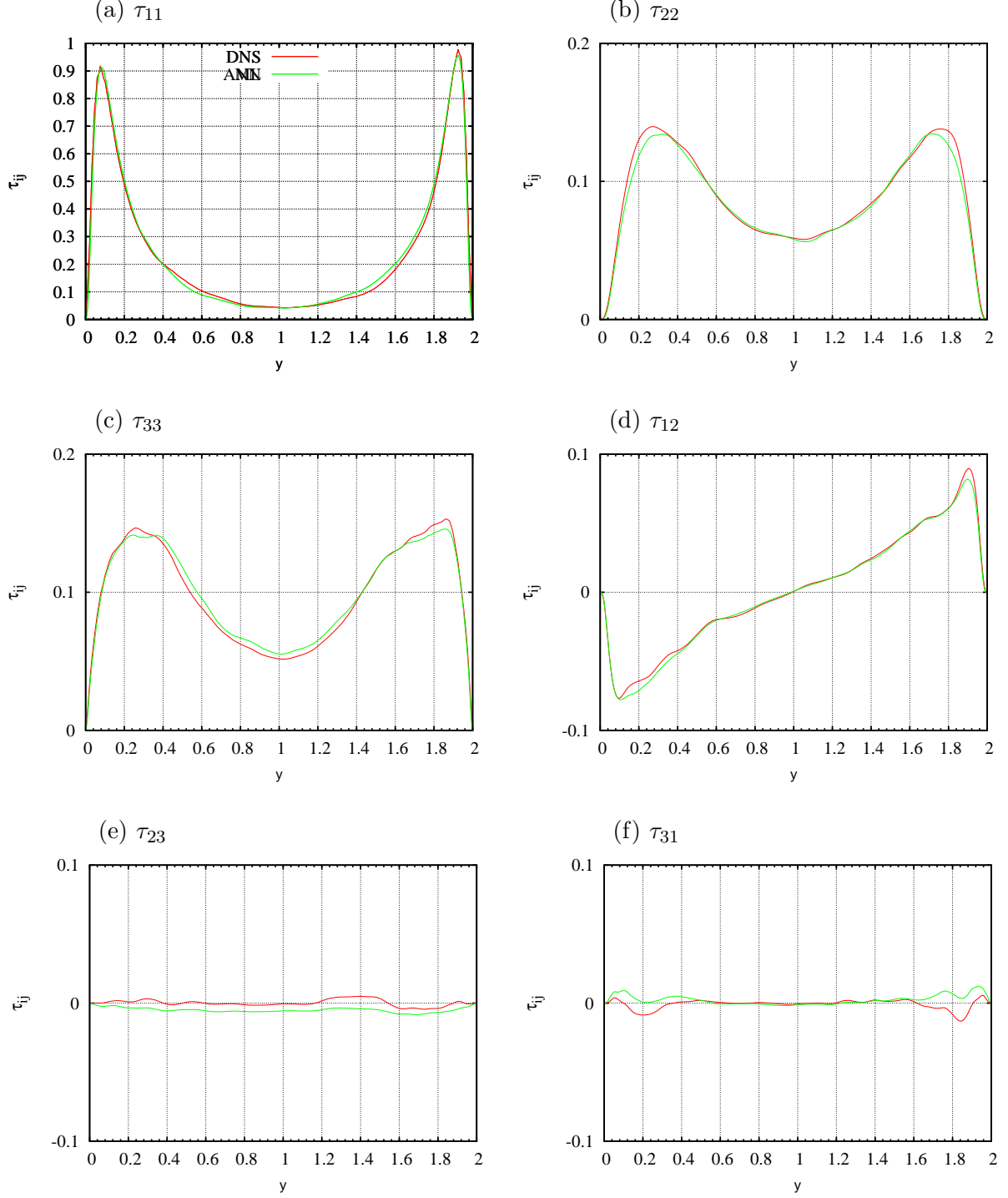


FIG. 7: SGS stress averaged in streamwise and spanwise directions. Comparison between  $\tau_{ij}^{(DNS)}$  and  $\tau_{ij}^{(ANN)}$ .  $Re_\tau = 180, (\overline{\Delta x}^+, \overline{\Delta y}_{\max}^+, \overline{\Delta z}^+) = (35.3, 9.9, 17.7)$ .

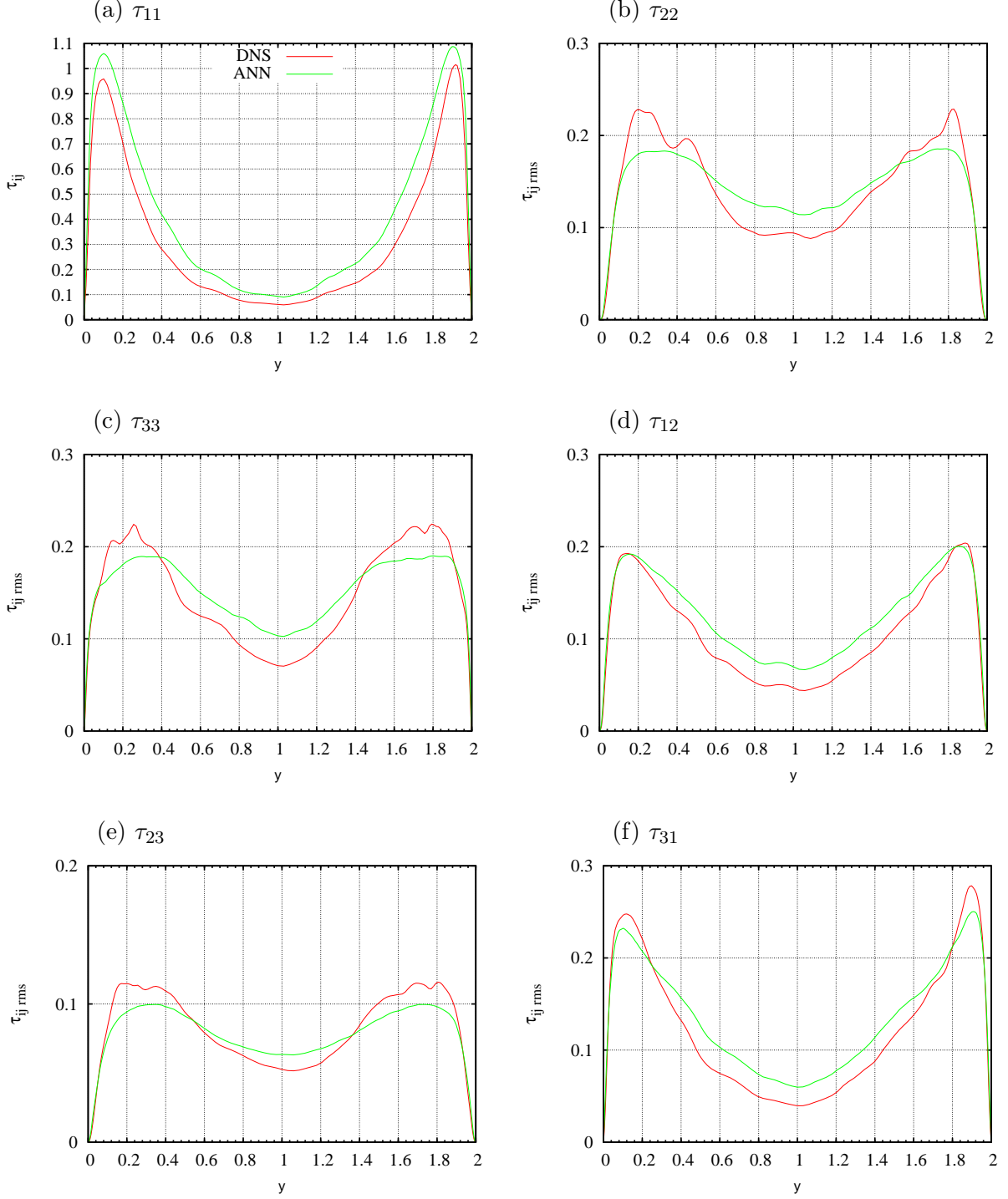


FIG. 8: Rms amplitude of fluctuation of SGS stress in streamwise and spanwise directions. Comparison between  $\tau_{ij}^{(DNS)}$  and  $\tau_{ij}^{(ANN)}$ .  $Re_\tau = 180$ ,  $(\overline{\Delta x^+}, \overline{\Delta y_{\max}^+}, \overline{\Delta z^+}) = (35.3, 9.9, 17.7)$ .

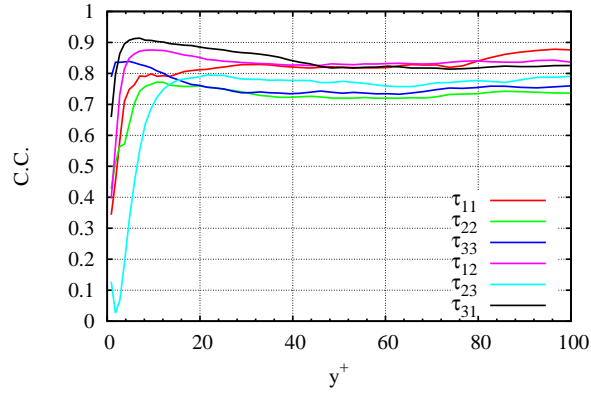


FIG. 9: Correlation coefficients between  $\tau_{ij}^{(DNS)}$  and  $\tau_{ij}^{(ANN)}$  near wall region. Correlation coefficients are averaged in streamwise and spanwise directions.

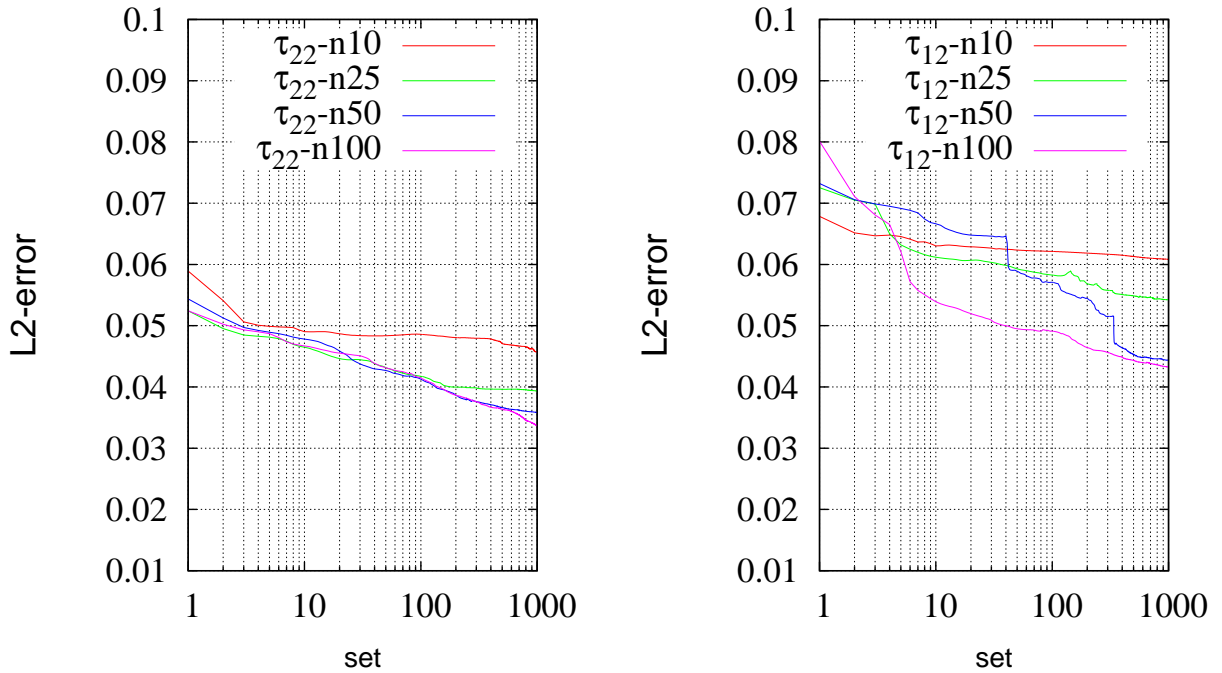


FIG. 10:  $L^2$ -norm of error between the output and the training target as a function of number of iterations. (Left)  $\tau_{12}$ , (right)  $\tau_{22}$ .

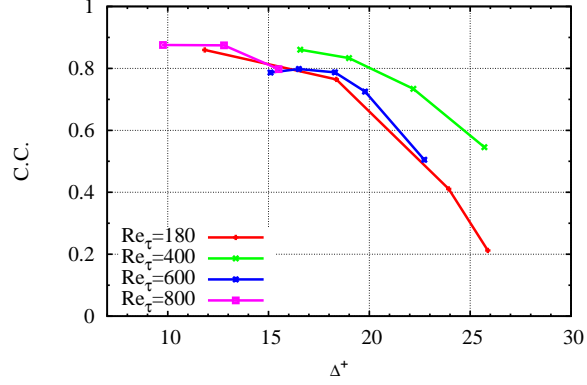


FIG. 11: Correlation coefficients between  $\tau_{ij}^{(DNS)}$  and  $\tau_{ij}^{(ANN)}$ . Dependence on the filter size. Correlation coefficients are averaged in the whole domain.

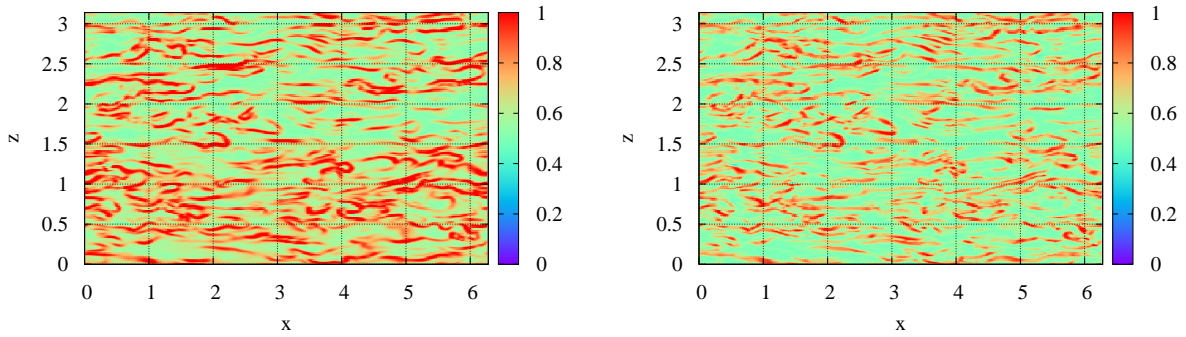


FIG. 12: Comparison between  $\tau_{11}^{(DNS)}$  obtained by filtering DNS data of  $Re_\tau = 400$  with filter size  $(\overline{\Delta x^+}, \overline{\Delta y_{\max}^+}, \overline{\Delta z^+}) = (34.3, 17.9, 17.5)$  and  $\tau_{11}^{(ANN)}$  predicted by ANN trained at  $Re_\tau = 180$  with filter size  $(\overline{\Delta x^+}, \overline{\Delta y_{\max}^+}, \overline{\Delta z^+}) = (35.3, 9.9, 17.7)$ .  $y = 0.1$ .

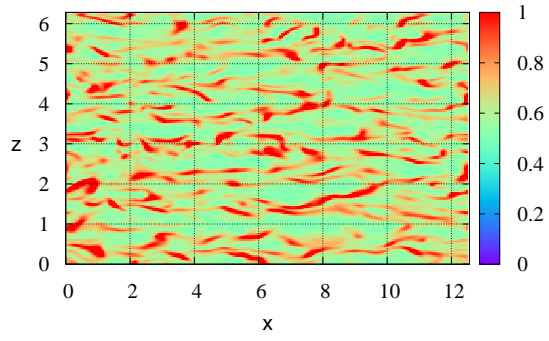


FIG. 13: Distribution of  $\tau_{11}$  obtained by gradient model.  $Re_\tau = 180$ ,  
 $(\overline{\Delta x^+}, \overline{\Delta y_{\max}^+}, \overline{\Delta z^+}) = (35.3, 9.9, 17.7)$ .